Determination of the parameters of the triaxial earth ellipsoid as derived from present-day geospatial techniques

Tomás Soler

National Geodetic Survey (NGS), National Oceanic and Atmospheric Administration (NOAA), Retired. 13510 Flowerfield Drive, Potomac, MD 20854, USA. Email: tomsolerngs@gmail.com

Jen-Yu Han (corresponding author)

Department of Civil Engineering, National Taiwan University. 1, Sec. 4, Roosevelt Rd., Taipei 10617, Taiwan. Email: jyhan@ntu.edu.tw

Abstract. This investigation implements a least-squares methodology to fit a triaxial ellipsoid to a set of three-dimensional Cartesian coordinates obtained from present-day geospatial techniques, materializing the terrestrial frame ITRF2014. To approximate, as much as possible previous research on this topic, the original spatial values of the station coordinates were "reduced" to the surface of the EGM2008 geoid model by introducing a simple and straightforward procedure. The mathematical model adopted in all LS solutions is the standard quadric polynomial equation parameterizing a triaxial ellipsoid. Functionally related to these polynomial coefficients are nine geometric parameters: the three ellipsoid semi-axes, its origin location with respect to the current conventional geocentric terrestrial frame, and the three rotations defining its spatial orientation. The final results are compatible with the pioneering work started by Burša in 1970 and, lately, by a recent publication by Panou and colleagues in that incorporates updated geoid models.

Keywords: triaxial ellipsoid fitting; ITRF2014 coordinates; geoid model EGM2008; least-squares solution

Declarations:

Funding (Not applicable)

Conflicts of interest/Competing interests (Not applicable)

Availability of data and material (Not applicable)

Code availability (Not applicable)

Introduction

Leaving aside the convenience or not of adopting a triaxial ellipsoid as a replacement to the two-parameter rotational ellipsoid GRS80 presently adopted by the International Association of Geodesy (Moritz 1992), scientists have calculated, using different initial assumptions, the parameters of a supposedly best-fitting triaxial earth ellipsoid. Table 1 shows, chronologically, the most recent set of semi-axis values ($\bar{a}$, $\bar{b}$, $\bar{c}$) that different authors have published to date to specify the size and shape of a presumed triaxial earth ellipsoid. Krasovsky, also known as Krassovsky and Krasovski, mainly published all his work in Russian. His results of 1902 and 1972, were cited in the English geodetic literature by Zhuravlev (1972) and Geodetic Glossary (1986). The tabulated quantities credited to Eitschberger were recently recounted by Grafarend et al. (2014). Finally, Panou et al. (2020) report a myriad of solutions; their values in Table 1 correspond to the solution derived from the EGM2008 (Earth Gravimetric Earth Model of 2008) geoid model (Pavlis et al. 2012). The final listed triaxial ellipsoid determined by Soler and Han, also based on EGM2008, is presented herein for the first time.

Table 1. Semi-axes of some published triaxial earth ellipsoids

	$\bar{a}$ (m)	$\bar{b}$ (m)	$\bar{c}$ (m)
Krasovsky (1902)	6378250.	6378050.	6356730.
Krasovsky (1972)	6378245.	6378033.	6356863.019

Schliephake (1956)	6378245.	6378032.4	6356863.0
Burša (1970)	$6378173. \pm 10$	$6378105. \pm 16.21$	$6356754. \pm 10.01$
Eitschberger (1978)	6378173.43	6378103.9	6356754.4
Panou et al.(2020)	6378171.88 ± 0.06	6378102.03 ± 0.06	6356752.24 ± 0.06
Soler and Han (Table 3)	6378187.20 ± 3.97	6378092.31 ± 3.92	6356763.60 ± 3.78

It should be mentioned here that triaxial ellipsoids are often used in planetology to represent mathematical models of celestial bodies; e.g., Drummond and Christou (2008), Diaz-Toca et al. (2019) where a few examples identifying the corresponding sources are tabulated. However, normally only the three semi-axes of the triaxial ellipsoid are provided and rarely do they include attached standard deviations. Notice that in Table 1 only a few lines include uncertainties. Incidentally, Burša (1970) provides the semi-major axis ($\bar{a}$) and two eccentricities (e and e_1) with their corresponding standard deviations. These known values were transformed before inserting them in Table 1 after making use of the following well-established conventional formulation:

$$\bar{b} = \bar{a}\sqrt{1-e^2} \quad \text{and} \quad \sigma_{\bar{b}}^2 = \left(\frac{\partial \bar{b}}{\partial \bar{a}}\right)^2 \sigma_{\bar{a}}^2 + \left(\frac{\partial \bar{b}}{\partial e^2}\right)^2 \sigma_{e^2}^2 = (1-e^2)\sigma_{\bar{a}}^2 + \frac{\bar{a}^2}{4(1-e^2)}\sigma_{e^2}^2 \qquad (1)$$

that assumes no correlations between the semi-major axis $\bar{a}$ and eccentricity e.

Similar equations apply to the semi-minor axis $\bar{c} = \bar{a}\sqrt{1-e_1^2}$. By the way, these values were revised on several occasions in Burša (1971), Burša and Pícha (1972), Burša and Šíma (1980) and Burša and Fialová (1993). These alternative solutions are tabulated in Panou et al. (2020). However, the differences with respect to his very first determination, considered by most scientists to be the gold standard for the triaxial earth, are not significant in the context of this investigation.

Methodology

The methodology describing in detail the mathematical theory executed to achieve the final results presented in this document was recently published in Soler et al. (2020). However, to facilitate the full comprehension of the particulars by the reader, the primary steps contained in the process will be briefly described below to make the narrative self-inclusive:

1) The original LS mathematical model is the standard quadric polynomial equation parameterizing the definition of the surface of a triaxial ellipsoid, namely (see e.g. Bektaş 2014, 2015; Soler et al. 2020),

$$F(x,y,z) = a\,x^2 + b\,y^2 + c\,z^2 + 2d\,xy + 2e\,xz + 2f\,yz + 2g\,x + 2h\,y + 2i\,z - 1 = 0 \qquad (2)$$

The coefficients a, b, c, .. i are the parameters to be solved for, while the (x, y, z) coordinates at each point are the observations to which the triaxial ellipsoid surface is fitted to.

2) Once the polynomial coefficients and their variance-covariance matrix are known they are transformed into the nine geometric constants defining the size and shape of the triaxial ellipsoid, mainly, the three semi-axes $(\bar{a}, \bar{b}, \bar{c})$, the coordinates of the origin of the ellipsoid with respect to the (x, y, z) frame and, finally, the counterclockwise rotations about the three ellipsoid axes (x_E, y_E, z_E) to make it parallel to the terrestrial frame (x, y, z). The complete procedure was unambiguously explained in Soler et al. (2020) following some of the ideas presented in Bektaş (2014).

3) Finally, the variance-covariance (v-c) matrices for the nine ellipsoidal parameters are computed. This is the most intricate calculation of the three steps. Principally, because it involves the determination of the v-c matrices of three eigenvalues and six eigenvectors applying the procedure originally introduced in Soler and van Gelder (1991, 2006) and later expanded and improved in Han et al. (2007). Considering that the typical reader may not be familiar with the practical implementation of this process, the mathematical background required to accomplish this specific goal will be succinctly covered.

Recall that as a byproduct of the LS solution, the v-c matrix of the nine polynomial coefficients denoted as $[\Sigma]_{(a,b,c,\dots,i)}$, is known. With this in mind, the complete solution of the problem is described in the following two subsections.

Variance-covariance matrix of the origin of the ellipsoid

The coordinates of the origin of the ellipsoid can be computed using the following matrix equation (Soler et al. 2020):

$$\begin{Bmatrix} x_0 \\ y_0 \\ z_0 \end{Bmatrix} = -\begin{bmatrix} a & d & e \\ d & b & f \\ e & f & c \end{bmatrix}^{-1} \begin{Bmatrix} g \\ h \\ i \end{Bmatrix} = \frac{-1}{abc + 2dfe - be^2 - af^2 - cd^2} \begin{bmatrix} bc - f^2 & -cd + ef & df - be \\ -cd + ef & ac - e^2 & -af + de \\ df - be & -af + de & ab - d^2 \end{bmatrix} \begin{Bmatrix} g \\ h \\ i \end{Bmatrix} \tag{3}$$

The above equation shows that if the polynomial coefficients g, h, and i are equal to zero in (2) the ellipsoid is centered at the origin of the (x, y, z) reference frame. Otherwise, by standard propagation of errors, one has:

$$[\Sigma]_{(x_0,y_0,z_0)} = [J][\Sigma]_{(a,b,c\dots i)}[J]^T \tag{4}$$

where the mathematical expression for the Jacobian matrix $\underset{3\times 9}{[J]} = \left[\frac{\partial(x_0, y_0, z_0)}{\partial(a,b,c\dots i)}\right]$ was given explicitly in (46) of Soler et al. (2020).

Variance-covariance matrices of the semi-axes and rotations

A symmetric matrix $[S]$ is constructed having the following value:

$$[S] = \begin{bmatrix} s_{11} & s_{12} & s_{13} \\ s_{21} & s_{22} & s_{23} \\ s_{31} & s_{32} & s_{33} \end{bmatrix} = -\frac{1}{F(x_0, y_0, z_0)} \begin{bmatrix} a & d & e \\ d & b & f \\ e & f & c \end{bmatrix} \tag{5}$$

Notice that $F(x_0, y_0, z_0)$ is equal to a scalar that results from particularizing (2) to the coordinates of the origin of the ellipsoid (thus, it is also a function of variables a, b, c, ….i). Thus, one can immediately arrange the six distinct elements of the symmetric matrix [S] as a column vector, essentially:

$$\begin{Bmatrix} s_{11} \\ s_{22} \\ s_{33} \\ s_{21} \\ s_{31} \\ s_{32} \end{Bmatrix} = -\frac{1}{F(x_0, y_0, z_0)} \begin{Bmatrix} a \\ b \\ c \\ d \\ e \\ f \end{Bmatrix} = \begin{Bmatrix} \mathsf{F}_1(a,b,c,...,i) \\ \mathsf{F}_2(a,b,c,...,i) \\ \mathsf{F}_3(a,b,c,...,i) \\ \mathsf{F}_4(a,b,c,...,i) \\ \mathsf{F}_5(a,b,c,...,i) \\ \mathsf{F}_6(a,b,c,...,i) \end{Bmatrix} \tag{6}$$

The v-c matrix of these six elements can be obtained by calculating the following matrix equation:

$$[\Sigma]_{(s_{11}, s_{22}, ..., s_{32})} = [\mathsf{J}][\Sigma]_{(a,b,c,...,i)}[\mathsf{J}]^T \tag{7}$$

where the Jacobian $\underset{6\times 9}{[\mathsf{J}]} = \left[\frac{\partial(\mathsf{F}_1, \mathsf{F}_2, ..., \mathsf{F}_6)}{\partial(a,b,c,...,i)}\right]$ computed from (6) was given explicitly by (52) in Soler et al. (2020).

By eigen-decomposition theory, the symmetric matrix $[S]$ takes the form:

$$[S] = [E]^T[\Lambda][E] \tag{8}$$

where

$$[E] = \begin{bmatrix} \vec{e}_1 \\ \cdots \\ \vec{e}_2 \\ \cdots \\ \vec{e}_3 \end{bmatrix} = \begin{bmatrix} e_{11} & e_{12} & e_{13} \\ e_{21} & e_{22} & e_{23} \\ e_{31} & e_{32} & e_{33} \end{bmatrix} \tag{9}$$

contains the three eigenvectors (row vectors) and $[\Lambda]$ is the diagonal matrix

$$[\Lambda] = \begin{bmatrix} \lambda_1 & 0 & 0 \\ 0 & \lambda_2 & 0 \\ 0 & 0 & \lambda_3 \end{bmatrix} \tag{10}$$

where λ_1, λ_2 and λ_3 are the three eigenvalues of the matrix $[S]$. Then, the three semi-axes of the triaxial ellipsoid are defined by the equations:

$$\bar{a} = \frac{1}{\sqrt{\lambda_1}},\ \bar{b} = \frac{1}{\sqrt{\lambda_2}},\ \bar{c} = \frac{1}{\sqrt{\lambda_3}} \tag{11}$$

Furthermore, the three rotation (counterclockwise positive) angles, respectively around the semi-major, semi-middle and semi-minor axes, are computed as a function of the eigenvectors using the expressions:

$$\varepsilon_1 = \tan^{-1}\left(\frac{-e_{32}}{e_{33}}\right), \quad \varepsilon_2 = \sin^{-1}\left(e_{31}\right), \quad \varepsilon_3 = \tan^{-1}\left(\frac{-e_{21}}{e_{11}}\right) \tag{12}$$

The v-c matrix of the eigenvalues and eigenvectors of a 3×3 symmetric matrix such as $[S]$ will be denoted here as $[\Sigma]_{(\lambda_1,\lambda_2,\lambda_3,vec[E])}$ where $vec[E] = \{e_{11}, e_{21}, e_{31}, \ldots, e_{33}\}^T$ or explicitly:

$$[\Sigma]_{(\lambda_1,\lambda_2,\lambda_3,vec[E])} = \left[\begin{array}{c:c} \underset{3\times3}{[\Sigma]_{(\lambda_1,\lambda_2,\lambda_3)}} & \underset{3\times9}{[\bullet]} \\ \hdashline \underset{9\times3}{[\bullet]^T} & \underset{9\times9}{[\Sigma]_{(e_{11},e_{21},e_{31},\ldots,e_{33})}} \end{array}\right]$$

$$= \left[\begin{array}{ccc:ccccccccc}
\sigma^2_{\lambda_1} & \sigma_{\lambda_1\lambda_2} & \sigma_{\lambda_1\lambda_3} & \sigma_{\lambda_1 e_{11}} & \sigma_{\lambda_1 e_{21}} & \sigma_{\lambda_1 e_{31}} & \sigma_{\lambda_1 e_{12}} & \sigma_{\lambda_1 e_{22}} & \sigma_{\lambda_1 e_{32}} & \sigma_{\lambda_1 e_{13}} & \sigma_{\lambda_1 e_{23}} & \sigma_{\lambda_1 e_{33}} \\
 & \sigma^2_{\lambda_2} & \sigma_{\lambda_2\lambda_3} & \sigma_{\lambda_2 e_{11}} & \sigma_{\lambda_2 e_{21}} & \sigma_{\lambda_2 e_{31}} & \sigma_{\lambda_2 e_{12}} & \sigma_{\lambda_2 e_{22}} & \sigma_{\lambda_2 e_{32}} & \sigma_{\lambda_2 e_{13}} & \sigma_{\lambda_2 e_{23}} & \sigma_{\lambda_2 e_{33}} \\
 & & \sigma^2_{\lambda_3} & \sigma_{\lambda_3 e_{11}} & \sigma_{\lambda_3 e_{21}} & \sigma_{\lambda_3 e_{31}} & \sigma_{\lambda_3 e_{12}} & \sigma_{\lambda_3 e_{22}} & \sigma_{\lambda_3 e_{32}} & \sigma_{\lambda_3 e_{13}} & \sigma_{\lambda_3 e_{23}} & \sigma_{\lambda_3 e_{33}} \\
\hdashline
 & & & \sigma^2_{e_{11}} & \sigma_{e_{11}e_{21}} & \sigma_{e_{11}e_{31}} & \sigma_{e_{11}e_{12}} & \sigma_{e_{11}e_{22}} & \sigma_{e_{11}e_{32}} & \sigma_{e_{11}e_{13}} & \sigma_{e_{11}e_{23}} & \sigma_{e_{11}e_{33}} \\
 & & & & \sigma^2_{e_{21}} & \sigma_{e_{21}e_{31}} & \sigma_{e_{21}e_{12}} & \sigma_{e_{21}e_{22}} & \sigma_{e_{21}e_{32}} & \sigma_{e_{21}e_{13}} & \sigma_{e_{21}e_{23}} & \sigma_{e_{21}e_{33}} \\
 & & & & & \sigma^2_{e_{31}} & \sigma_{e_{31}e_{12}} & \sigma_{e_{31}e_{22}} & \sigma_{e_{31}e_{32}} & \sigma_{e_{31}e_{13}} & \sigma_{e_{31}e_{23}} & \sigma_{e_{31}e_{33}} \\
 & & & & & & \sigma^2_{e_{12}} & \sigma_{e_{12}e_{22}} & \sigma_{e_{12}e_{32}} & \sigma_{e_{12}e_{13}} & \sigma_{e_{12}e_{23}} & \sigma_{e_{12}e_{33}} \\
 & & & & & & & \sigma^2_{e_{22}} & \sigma_{e_{22}e_{32}} & \sigma_{e_{22}e_{13}} & \sigma_{e_{22}e_{23}} & \sigma_{e_{22}e_{33}} \\
 & & & & & & & & \sigma^2_{e_{32}} & \sigma_{e_{32}e_{13}} & \sigma_{e_{32}e_{23}} & \sigma_{e_{32}e_{33}} \\
 & & & & & & & & & \sigma^2_{e_{13}} & \sigma_{e_{13}e_{23}} & \sigma_{e_{13}e_{33}} \\
 & & & & & & & & & & \sigma^2_{e_{23}} & \sigma_{e_{23}e_{33}} \\
sym. & & & & & & & & & & & \sigma^2_{e_{33}}
\end{array}\right] \tag{13}$$

Note that this is a full symmetric matrix that contains the variances of the eigenvalues and eigenvectors along the diagonal, the covariances of the eigenvalues and eigenvectors (non-diagonal elements on the 3×3 and 9×9 diagonal blocks) and the cross-covariances of the eigenvalues and eigenvectors (non-diagonal blocks). For the purpose of this investigation, only the variances of the eigenvalues and eigenvectors are of interest.

The analytical way of how to compute the variance-covariance matrix of the eigenvalues and eigenvectors of a general 3×3 symmetric matrix, to the authors' knowledge, was first shown in Soler and van Gelder (1991, 2006) and later extended and enhanced in Han et al. (2007). This sought-after objective is accomplished through the following propagation of the error matrix equation

$$[\Sigma]_{(\lambda_1,\lambda_2,\lambda_3,vec[E])} = [K][\Sigma]_{(s_{11},s_{22},\ldots,s_{32})}[K]^T \tag{14}$$

where

$$\underset{12\times 6}{[K]} = \begin{bmatrix} \underset{3\times3}{[I]} & \underbrace{[0]}_{3\times3} \\ \underbrace{[0]}_{9\times3} & -\square\underbrace{\underset{3\times3}{[I]}\otimes\underset{3\times3}{[E]}}_{9\times9}\square\underset{9\times3}{[D_\Omega]} \end{bmatrix} \square \overbrace{\underset{6\times9}{[D_E]}\square\underbrace{\underset{3\times3}{[E]^T}\square\ \underset{3\times3}{[E]^T}}_{9\times3} \vdots -\square\underset{9\times9}{[D_S]}+\underset{9\times9}{[I]}\square\square\underbrace{\underset{3\times3}{[I]}\otimes\underset{3\times3}{[S]}}_{9\times9}\square\underset{9\times3}{[D_\Omega]}\square}^{6\times6} \square^{-1} \tag{15}$$

The symbol $\otimes$ denotes the Kronecker Product, defined by $[A]\otimes[B] = [a_{ij}[B]]$ if $[A] = [a_{ij}]$. The symbol $\square$ denotes the Khatri–Rao product defined by $[A] \square [B] = [A_1 \otimes B_1, \ldots, A_p \otimes B_p]$ if $[A_j]$ and $[B_j]$ ($j = 1, \ldots, p$) are (column) partitioned matrices of [A] and [B], respectively (see Rao & Mitra 1971, pp. 12–13 and the illustration in the Appendix). The matrices $[D_E]$, $[D_S]$ and $[D_\Omega]$ were explicitly given in Han et al. (2007) as

$$
\underset{6\times 9}{[D_E]} = \left[\begin{array}{ccc|ccc|ccc} 1 & 0 & 0 & 0 & 0 & 0 & 0 & 0 & 0 \\ 0 & 0 & 0 & 0 & 1 & 0 & 0 & 0 & 0 \\ 0 & 0 & 0 & 0 & 0 & 0 & 0 & 0 & 1 \\ \hline 0 & 0.5 & 0 & 0.5 & 0 & 0 & 0 & 0 & 0 \\ 0 & 0 & 0.5 & 0 & 0 & 0 & 0.5 & 0 & 0 \\ 0 & 0 & 0 & 0 & 0 & 0.5 & 0 & 0.5 & 0 \end{array}\right]; \quad \underset{9\times 9}{[D_S]} = \left[\begin{array}{ccc|ccc|ccc} 1 & 0 & 0 & 0 & 0 & 0 & 0 & 0 & 0 \\ 0 & 0 & 0 & 1 & 0 & 0 & 0 & 0 & 0 \\ 0 & 0 & 0 & 0 & 0 & 0 & 1 & 0 & 0 \\ \hline 0 & 1 & 0 & 0 & 0 & 0 & 0 & 0 & 0 \\ 0 & 0 & 0 & 0 & 1 & 0 & 0 & 0 & 0 \\ 0 & 0 & 0 & 0 & 0 & 0 & 0 & 1 & 0 \\ \hline 0 & 0 & 1 & 0 & 0 & 0 & 0 & 0 & 0 \\ 0 & 0 & 0 & 0 & 0 & 1 & 0 & 0 & 0 \\ 0 & 0 & 0 & 0 & 0 & 0 & 0 & 0 & 1 \end{array}\right]; \quad \underset{9\times 3}{[D_\Omega]} = \left[\begin{array}{ccc} 0 & 0 & 0 \\ 0 & 0 & -1 \\ 0 & 1 & 0 \\ \hline 0 & 0 & 1 \\ 0 & 0 & 0 \\ -1 & 0 & 0 \\ \hline 0 & -1 & 0 \\ 1 & 0 & 0 \\ 0 & 0 & 0 \end{array}\right]
$$

……….(16)

Once the values of the v-c matrix of eigenvalues and eigenvectors $\Sigma_{(\lambda_1,\lambda_2,\lambda_3,vec[E])}$ is known, the final v-c matrices of the semi-axes and rotations is given by

$$
\underset{6\times 6}{\Sigma}_{(\bar{a},\bar{b},\bar{c},\varepsilon_1,\varepsilon_2,\varepsilon_3)} = \underset{6\times 12}{[\mathsf{J}]} \underset{12\times 12}{\Sigma}_{(\lambda_1,\lambda_2,\lambda_3,vec[E])} \underset{12\times 6}{[\mathsf{J}]}^T \tag{17}
$$

and

$$
\underset{6\times 12}{[\mathsf{J}]} = \frac{\partial(\bar{a},\bar{b},\bar{c},\varepsilon_1,\varepsilon_2,\varepsilon_3)}{\partial(\lambda_1,\lambda_2,\lambda_3,vec[E])} = \begin{bmatrix} \frac{\partial\bar{a}}{\partial\lambda_1} & \frac{\partial\bar{a}}{\partial\lambda_2} & \frac{\partial\bar{a}}{\partial\lambda_3} & \frac{\partial\bar{a}}{\partial e_{11}} & \frac{\partial\bar{a}}{\partial e_{21}} & \frac{\partial\bar{a}}{\partial e_{31}} & \frac{\partial\bar{a}}{\partial e_{12}} & \frac{\partial\bar{a}}{\partial e_{22}} & \frac{\partial\bar{a}}{\partial e_{32}} & \frac{\partial\bar{a}}{\partial e_{13}} & \frac{\partial\bar{a}}{\partial e_{23}} & \frac{\partial\bar{a}}{\partial e_{33}} \\ \frac{\partial\bar{b}}{\partial\lambda_1} & \frac{\partial\bar{b}}{\partial\lambda_2} & \frac{\partial\bar{b}}{\partial\lambda_3} & \frac{\partial\bar{b}}{\partial e_{11}} & \frac{\partial\bar{b}}{\partial e_{21}} & \frac{\partial\bar{b}}{\partial e_{31}} & \frac{\partial\bar{b}}{\partial e_{12}} & \frac{\partial\bar{b}}{\partial e_{22}} & \frac{\partial\bar{b}}{\partial e_{32}} & \frac{\partial\bar{b}}{\partial e_{13}} & \frac{\partial\bar{b}}{\partial e_{23}} & \frac{\partial\bar{b}}{\partial e_{33}} \\ \frac{\partial\bar{c}}{\partial\lambda_1} & \frac{\partial\bar{c}}{\partial\lambda_2} & \frac{\partial\bar{c}}{\partial\lambda_3} & \frac{\partial\bar{c}}{\partial e_{11}} & \frac{\partial\bar{c}}{\partial e_{21}} & \frac{\partial\bar{c}}{\partial e_{31}} & \frac{\partial\bar{c}}{\partial e_{12}} & \frac{\partial\bar{c}}{\partial e_{22}} & \frac{\partial\bar{c}}{\partial e_{32}} & \frac{\partial\bar{c}}{\partial e_{13}} & \frac{\partial\bar{c}}{\partial e_{23}} & \frac{\partial\bar{c}}{\partial e_{33}} \\ \frac{\partial\varepsilon_1}{\partial\lambda_1} & \frac{\partial\varepsilon_1}{\partial\lambda_2} & \frac{\partial\varepsilon_1}{\partial\lambda_3} & \frac{\partial\varepsilon_1}{\partial e_{11}} & \frac{\partial\varepsilon_1}{\partial e_{21}} & \frac{\partial\varepsilon_1}{\partial e_{31}} & \frac{\partial\varepsilon_1}{\partial e_{12}} & \frac{\partial\varepsilon_1}{\partial e_{22}} & \frac{\partial\varepsilon_1}{\partial e_{32}} & \frac{\partial\varepsilon_1}{\partial e_{13}} & \frac{\partial\varepsilon_1}{\partial e_{23}} & \frac{\partial\varepsilon_1}{\partial e_{33}} \\ \frac{\partial\varepsilon_2}{\partial\lambda_1} & \frac{\partial\varepsilon_2}{\partial\lambda_2} & \frac{\partial\varepsilon_2}{\partial\lambda_3} & \frac{\partial\varepsilon_2}{\partial e_{11}} & \frac{\partial\varepsilon_2}{\partial e_{21}} & \frac{\partial\varepsilon_2}{\partial e_{31}} & \frac{\partial\varepsilon_2}{\partial e_{12}} & \frac{\partial\varepsilon_2}{\partial e_{22}} & \frac{\partial\varepsilon_2}{\partial e_{32}} & \frac{\partial\varepsilon_2}{\partial e_{13}} & \frac{\partial\varepsilon_2}{\partial e_{23}} & \frac{\partial\varepsilon_2}{\partial e_{33}} \\ \frac{\partial\varepsilon_3}{\partial\lambda_1} & \frac{\partial\varepsilon_3}{\partial\lambda_2} & \frac{\partial\varepsilon_3}{\partial\lambda_3} & \frac{\partial\varepsilon_3}{\partial e_{11}} & \frac{\partial\varepsilon_3}{\partial e_{21}} & \frac{\partial\varepsilon_3}{\partial e_{31}} & \frac{\partial\varepsilon_3}{\partial e_{12}} & \frac{\partial\varepsilon_3}{\partial e_{22}} & \frac{\partial\varepsilon_3}{\partial e_{32}} & \frac{\partial\varepsilon_3}{\partial e_{13}} & \frac{\partial\varepsilon_3}{\partial e_{23}} & \frac{\partial\varepsilon_3}{\partial e_{33}} \end{bmatrix}
$$

$$
= \begin{bmatrix}
-\frac{1}{2}\lambda_1^{-3/2} & 0 & 0 & 0 & 0 & 0 & 0 & 0 & 0 & 0 & 0 & 0 \\
0 & -\frac{1}{2}\lambda_2^{-3/2} & 0 & 0 & 0 & 0 & 0 & 0 & 0 & 0 & 0 & 0 \\
0 & 0 & -\frac{1}{2}\lambda_3^{-3/2} & 0 & 0 & 0 & 0 & 0 & 0 & 0 & 0 & 0 \\
0 & 0 & 0 & 0 & 0 & 0 & 0 & 0 & \frac{-e_{33}}{\left(e_{32}^2+e_{33}^2\right)} & 0 & 0 & \frac{e_{32}}{\left(e_{32}^2+e_{33}^2\right)} \\
0 & 0 & 0 & 0 & 0 & \frac{1}{\sqrt{1-e_{31}^2}} & 0 & 0 & 0 & 0 & 0 & 0 \\
0 & 0 & 0 & \frac{e_{21}}{\left(e_{21}^2+e_{11}^2\right)} & \frac{-e_{11}}{\left(e_{21}^2+e_{11}^2\right)} & 0 & 0 & 0 & 0 & 0 & 0 & 0
\end{bmatrix} \tag{18}
$$

It should be noted that the nonlinearity of any LS process could always be a concern if a rigorous estimation is anticipated. Several authors have treated this topic at length (Teunissen 1989). The formulation to determine the degree of approximation involved depends on the second partial derivative of the design matrix. Using the values already published in our previous paper (Soler et al. 2020) it is immediately seen that $\left.\frac{\partial^2 F}{\partial\{x\}^2}\right|_{\{x\}_0,\{l\}_0} = \underset{n\times 9}{[\,0\,]}$. Consequently, the linearized first order approximation invoked in our LS solution is necessary and sufficient.

Summarizing, equations (3), (11) and (12) solve for the sought after nine triaxial ellipsoid parameters as a function of the values of the polynomial coefficients a, b, c, …, i which are the unknowns in the least-squares solution processing. The variance-covariance matrices of the ellipsoidal parameters are obtained, respectively by (4), and (17) all of them derived directly from the value of $[\Sigma]_{(a,b,c,\ldots,i)}$ computed originally from the LS procedure and the intermediate equations (7) and (14).

By the way, equations (14) and (15) provide the solution for obtaining the full variance-covariance matrix of the eigenvalues and eigenvectors of any 3×3 symmetric matrix which is given on its general form by (13).

Here is a final note related to this topic. A recent publication by Panou and Agatza-Balodimou (2020) elaborates on the advantages and disadvantages of the direct versus indirect (the one proposed herein) methodologies to estimate the variance-covariance of the parameters involved in the fitting of a triaxial ellipsoid. As we related in this work and in our previous publication (Soler et al. 2020), our main intent was to explain in detail to the reader how to compute the v-c matrix of the eigenvalues and eigenvectors of a 3×3 symmetric matrix. As far as the authors are aware of, this operation is impossible to be performed without introducing the Kronecker and Khatri-Rao products, which, by the way, are an important part of the matrix algebra arsenal. Furthermore, although the correlations between eigenvalues and eigenvectors is determined, the authors, nevertheless, concur with Panou and Agatza-Balodimou (2020) that the full set of correlations between the different parameters of the triaxial ellipsoid cannot be estimated through our step-by-step indirect procedure. To obtain the correlations between shifts and semi-axes and rotations one needs to use their direct approach.

Data used in the calculations

The original data are the Cartesian coordinates of the ITRF2014 geodetic stations and their corresponding standard deviations that were extracted from the Software INdependent EXchange Format (SINEX) files (IERS Message 103 2006) of the latest solutions disseminated by the IERS (International Earth Rotation and Reference Systems Service; see Altamimi et al. 2016). This information was used to obtain the values of the Cartesian coordinates along the ellipsoid height on the surface of the EGM2008 geoid model (Pavlis et al. 2012) according to the schematic illustration depicted in Fig. 1.

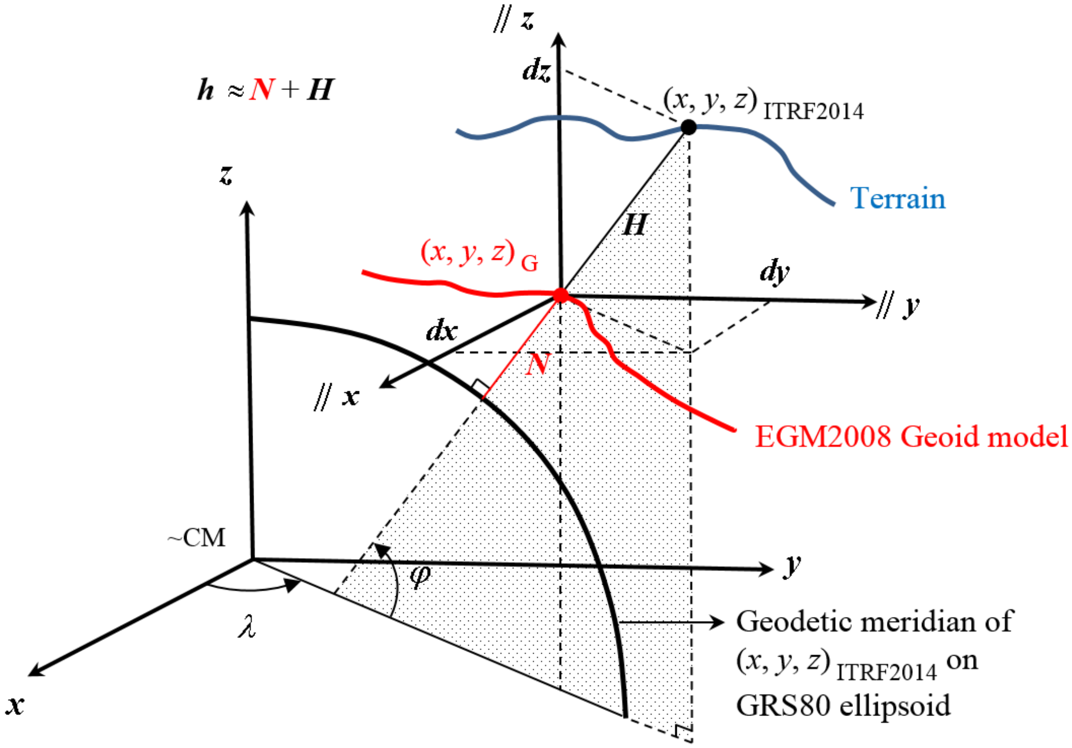

Fig. 1. Graphic relationship between different geodetic parameters

The triaxial ellipsoid is actually fitted to a cluster of $(x,y,z)_G$ coordinates, which in the example shown in Fig. 1 corresponds to the point of intersection between the ellipsoid height h and the geoid model EGM2008. Notice that the standard assumption $h \approx N + H$ was introduced. According to Fig. 1 one can write:

$$\begin{aligned}\begin{Bmatrix} x \\ y \\ z \end{Bmatrix}_G &= \begin{Bmatrix} x \\ y \\ z \end{Bmatrix}_{ITRF2014} - \begin{Bmatrix} dx \\ dy \\ dz \end{Bmatrix} = \begin{Bmatrix} x \\ y \\ z \end{Bmatrix}_{ITRF2014} - \begin{Bmatrix} \cos\lambda\cos\varphi H \\ \sin\lambda\cos\varphi H \\ \sin\varphi H \end{Bmatrix} \\ &= \begin{Bmatrix} x \\ y \\ z \end{Bmatrix}_{ITRF2014} - \begin{Bmatrix} \cos\lambda\cos\varphi(h-N) \\ \sin\lambda\cos\varphi(h-N) \\ \sin\varphi(h-N) \end{Bmatrix}\end{aligned} \tag{19}$$

Note the distinction between 3D coordinates of points referred to the ITRF2014 frame such as $(x, y, z)_G$ and coordinates of the stations belonging to the definition of the ITRF2014 frame: $(x, y, z)_{ITRF2014}$ (Altamimi et al. 2016).

In the above equation the value of h is rigorously known with respect to the GRS80 ellipsoid. On the other hand, the value of N could also be computed, at a certain level of accuracy, using the EGM2008 geoid model. In any event, the only errors affecting this "reduction" of the $(x, y, z)_{ITRF2014}$ coordinates to the value of $(x, y, z)_G$ on the surface of the geoid model are contained along the geodetic height and are mainly caused by the uncertainty on the value of N. Smaller errors, not affecting the final results, are introduced by the assumption that $h \approx N + H$

The 3D coordinates defining the ITRF20014 frame (Altamimi et al. 2016) which was initially used in this investigation, resulted from an accurate, up-to-date combination of four geospatial techniques: VLBI (Very Long Baseline Interferometry, Bachmann et al. 1915), GNSS (Global Navigation Satellite System, Rebischung et al 2016, SLR (Satellite Laser Ranging, Luceri and Pavlis (2016), and DORIS (Doppler Orbitography and Radiopositioning Integrated by Satellite, Moreaux et al. (2016). Thus, it should be considered the leading edge on the determination of accurate 3D geocentric Cartesian coordinates at a certain number of geodetic stations around the globe. From these sets of coordinates the values of $(x, y, z)_G$, see Fig. 1, "reduced" (downward continued) to the geoid were computed and used as available observations to which the sought triaxial ellipsoid was fitted.

The $(x, y, z)_{ITRF2014}$ coordinate data set was downloaded from the ITRF Website at the following URL address: http://itrf.ensg.ign.fr/ ITRF_solutions/2014/ITRF2014_files.php. All coordinates refer to the 2010.0027 epoch. The undulations of the EGM2008 geoid model, without accompanied statistics, were interactively accessible at the following Web platform with URL: https://geographiclib.sourceforge.io/cgi-bin/GeoidEval?input=39.35+-74.41666&option=Submit

Least Squares (LS) Solutions

Among all LS minimization options described in Soler et al. (2020) the so-called "general LS solution" was the strategy selected for the reasons outlined in that publication. It must be stressed that this sort of solution is based on a mathematical model, which is an implicit function of unknowns and observations schematically written as $F(X,L)=0$. However, the reader should be aware that in the specialized literature dedicated to the theory of least-squares, this functional relationship receives other names as, for example, "mixed adjustment model" in Leick et al. (2015). The unknowns X in this particular instance are the nine coefficients of equation (2) defining the quadric surface of the fitted triaxial ellipsoid, while the observations L is the set of 3D $(x,y,z)_G$ coordinates, which are also referred to the ITRF2014 frame although they are not part of the IERS ITRF2014 solution. Following the account in the methodology section presented previously, once the nine coefficients of the polynomial are known one is able to determine, using several sequential algebraic steps described previously, the corresponding nine parameters that fully define the triaxial ellipsoid in space, that is: three semi-axes $(\bar{a},\bar{b},\bar{c})$, the three shifts of its origin with respect to the ITRF2014 terrestrial frame (x_0,y_0,z_0) and, finally, the positive counterclockwise rotations $(\varepsilon_1,\varepsilon_2,\varepsilon_3)$ about a Cartesian frame initially coinciding with the semi-axes of the ellipsoid that is rotated to attain parallelism with the geocentric terrestrial frame. Lastly, after implementing a propagation of errors strategy explained in the section Methodology, their associated statistics for these nine parameters are also estimated.

LS solution fundamentals

Figure 2 depicts with dots the location of stations around the globe involved in the definition of the ITRF2014 frame. In contrast, denoted with small circles are shown the 1163 stations participating in the LS solution. This selected number of stations was used because the accurate errors of the geoid heights around the planet are not well-known; therefore, an upper limit for H was established and only stations with values of $H < 500$ m were used. This specific cutoff value was chosen to eliminate possible unknown errors on the modeled undulations of the geoid in mountainous regions were, by obvious reasons, it is more difficult to produce rigorous values of the geoid height. At the same time, the greater the value of H is, the larger the error that may disturb the approximation $h \approx N + H$ on account of the unpredictability of the curvature of the plumb line. Nonetheless, notice from Fig. 2 that an adequate coverage of ITRF2014 stations with the restriction $H < 500$ is scattered around the earth and dispersed to a great extent among the four quadrants of the planet. It should be emphasized once more that no values of the undulations of the EGM2008 geoid model were used as observations, although the knowledge of N at each station was required as an intermediate quantity to determine the 3D coordinates $(x, y, z)_G$, the actual observables to which the triaxial ellipsoid was fitted to. Precisely, this fact certainly makes the procedure implemented in this article to be markedly different to any other previous investigation that attempted to unravel the characteristics of the best triaxial ellipsoid parameters of an earth model. In the experiment elaborated here, the only errors in the position of the 3D points are counted along the geodetic height mainly due to uncertainties on the undulations, otherwise, the position of the coordinates of the observables in space are as rigorous as feasible.

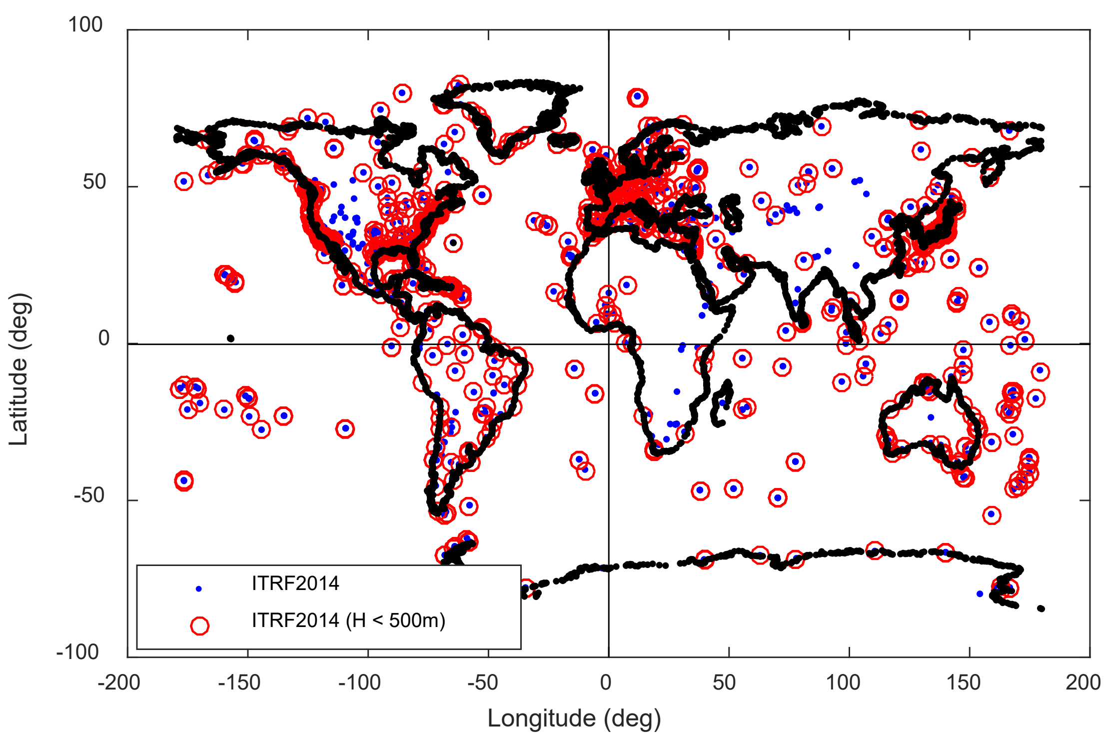

Fig. 2. Geographic distributions of the 1163 geodetic stations ($H < 500$ m) on the surface of the geoid used in the LS solution

Recall that the values of (λ, φ) shown in Fig. 1 are rigorously known with respect to the GRS80 reference ellipsoid, and with H they are merely used to determine the values of the coordinates $(x, y, z)_G$ in space. Once all ITRF20014 selected station was corrected by the displacement in Cartesian coordinates caused by the reduction to the geoid (see Fig. 1) and the coordinates $(x, y, z)_G$ were known, the LS procedure described above was implemented.

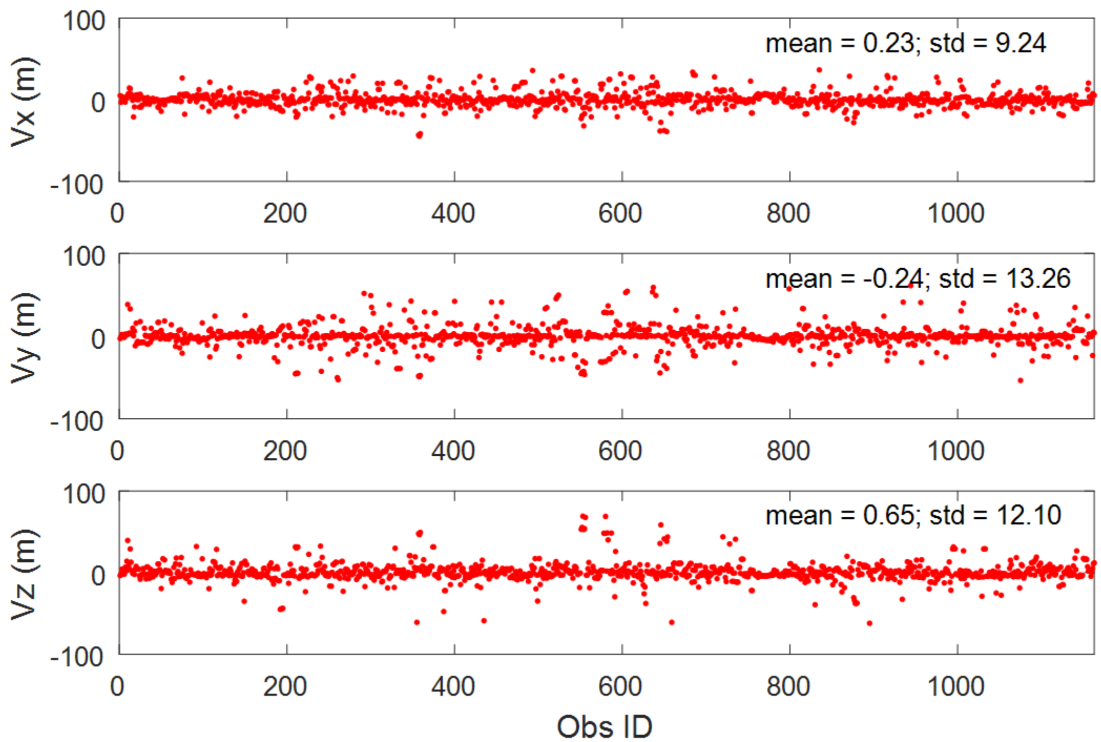

Fig. 3. Plot of the residuals (v_x, v_y, v_z) from the LS solution for the $(x, y, z)_G$ coordinates

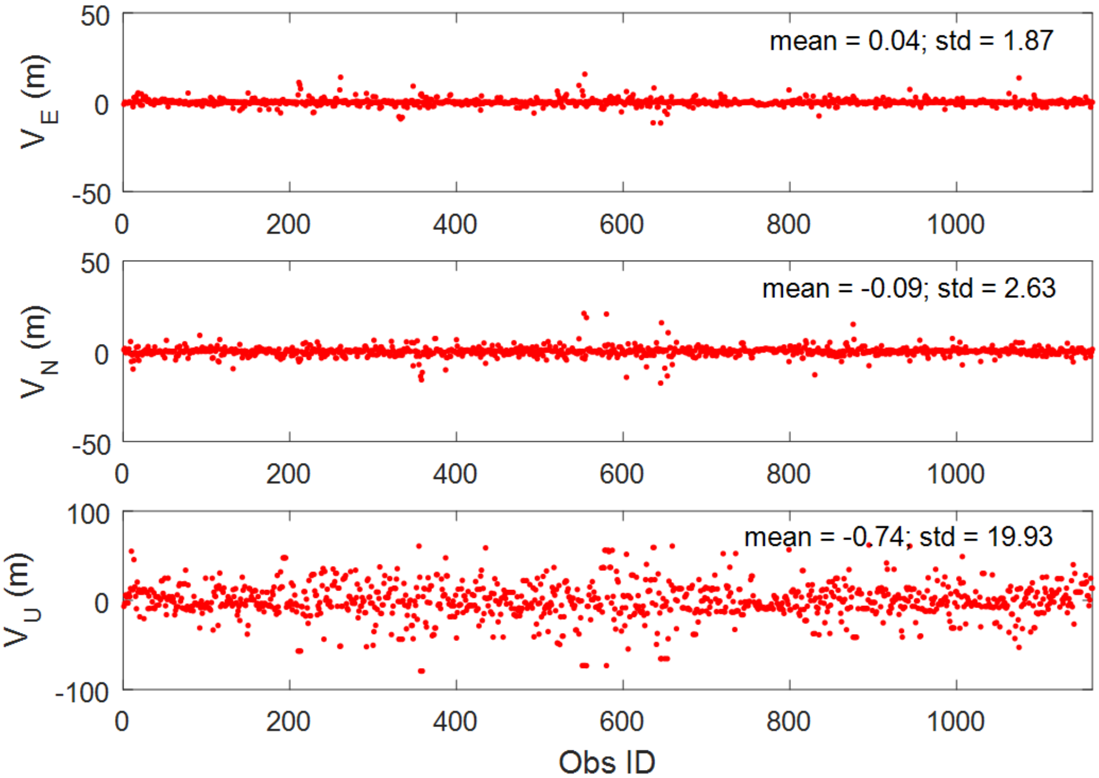

Fig. 4. Plot of the residuals along the local geodetic frame $(\boldsymbol{v}_E, \boldsymbol{v}_N, \boldsymbol{v}_U)$

The least-squares residual plots pertaining to each one of the used stations are available in Fig. 3, where it is clearly shown that all the residuals along the *x*, *y*, and *z* components is always between ± 100 m. Figure 4 shows the representation of the residuals of Fig. 3 transformed into the local (topocentric) geodetic: frame east, north, up (not shown in Fig. 1). This plot was created to approximately visualize the magnitude of the residuals along the geodetic height (up) component by implementing the well-known equation:

$$\begin{Bmatrix} v_E \\ v_N \\ v_U \end{Bmatrix} = \begin{bmatrix} -\sin\lambda & \cos\lambda & 0 \\ -\cos\lambda\sin\varphi & -\sin\lambda\sin\varphi & \cos\varphi \\ \cos\lambda\cos\varphi & \sin\lambda\cos\varphi & \sin\varphi \end{bmatrix} \begin{Bmatrix} v_x \\ v_y \\ v_z \end{Bmatrix} \tag{20}$$

As expected, the conversion of residuals from Cartesian to curvilinear coordinates shows that the geodetic height residual along the local frame v_U obviously presents the maximum scatter of the three residual components (v_E, v_N, v_U). Having said that, observe that according to Fig. 4, the resultant standard deviation of about 20 m for v_U definitely exhibits a reasonable triaxial ellipsoid fitting to the cluster of generated three-dimensional points $(x, y, z)_G$.

Results from the LS solutions

Table 2 presents the estimates of the nine coefficients of equation (2) resulting from the LS solution using the set of coordinates $(x, y, z)_G$ as observations with their corresponding standard deviations. The statistics in Table 2 resulted directly from the LS process and the assumption of a diagonal weight matrix extracted from the ITRF2014 SINEX file.

Table 2. Estimates of the parameters of the quadric equation of the fitted triaxial ellipsoid

Parameters	Estimates [$\times 10^{-13}$]
a	$0.24581357 \pm 0.00000016$
b	$0.24582046 \pm 0.00000014$
c	$0.24747303 \pm 0.00000015$
d	$0.00000124 \pm 0.00000010$
e	$-0.00000067 \pm 0.00000010$
f	$-0.00000119 \pm 0.00000010$
g	$-0.50342905 \pm 0.34889404$
h	$0.74081758 \pm 0.34570154$
i	$-1.86086692 \pm 0.32974988$
Root-mean-squared distances (m)	20.1977

Because the coefficients in Table 2 are difficult to interpret geometrically, the following step was to transform them into the parameters shown in Table 3 after following the algebraic operations described in the Methodology section. This table presents in column arrangement the resultant nine spatial parameters defining the geometric characteristics (see Fig. 5) of the triaxial ellipsoid mainly: the three shifts of the origin (x_0, y_0, z_0), three semi-axes $(\bar{a}, \bar{b}, \bar{c})$, and the three rotations $(\varepsilon_1, \varepsilon_2, \varepsilon_3)$ with accompanying standard deviations. The column on the left contains the results obtained from this investigation. The middle column tabulates the results published in Panou et al. (2020), and finally, the column on the right shows the original values reported by Burša (1970). The standard deviations in Table 3 resulted after a step-by-step procedure following a conventional propagation of errors strategy.

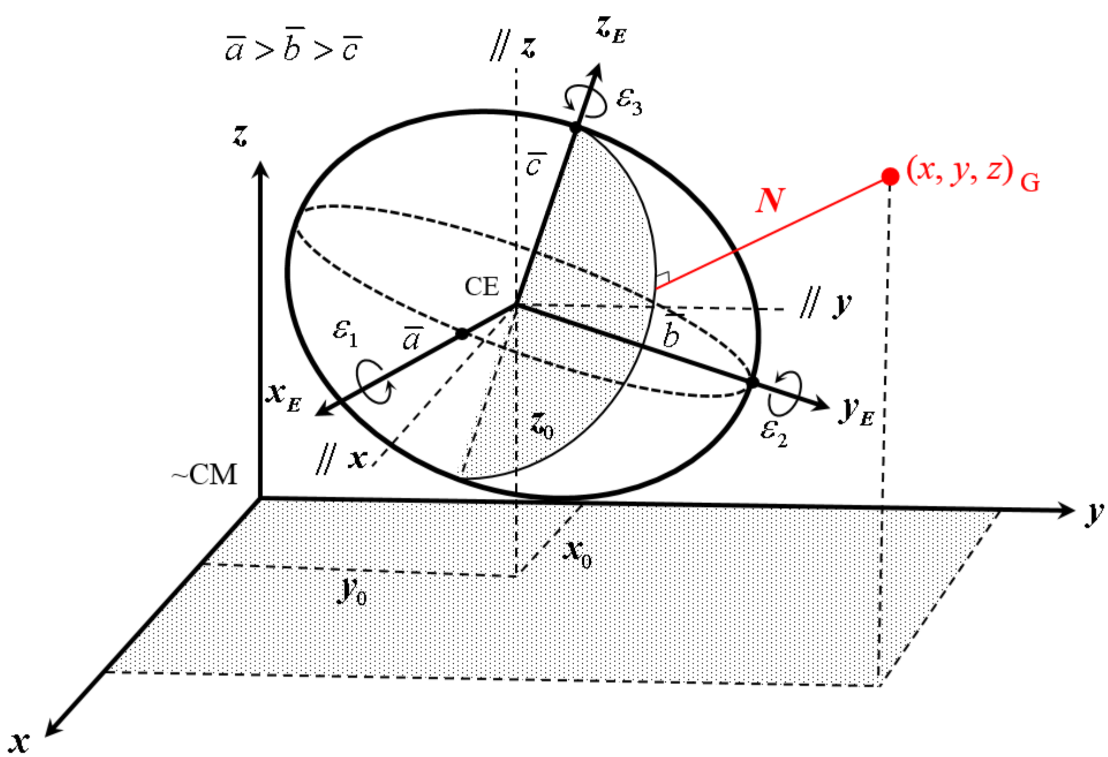

Fig. 5. Graphic depiction of the nine geometric parameters defining in space the best fitted triaxial ellipsoid

Table 3. Ellipsoidal parameters ($\pm 1\,\boldsymbol{\sigma}$) derived from the coefficients in Table 2

Parameters	This study	Panou et al.	Burša Ellipsoid
x_0 (m)	-2.05 $\pm$ 1.42		0
y_0 (m)	3.01 $\pm$ 1.41		0
z_0 (m)	7.52 $\pm$ 1.32		0
$\overline{a}$ (m)	6378187.20 $\pm$ 3.97	6378171.88 $\pm$ 0.06	6378173.00 $\pm$ 10.00
$\overline{b}$ (m)	6378092.31 $\pm$ 3.92	6378102.03 $\pm$ 0.06	6378105.15 $\pm$ 16.21
$\overline{c}$ (m)	6356763.60 $\pm$ 3.78	6356752.24 $\pm$ 0.06	6356754.36 $\pm$ 10.01
ε_1 (^{0})	-0.0447 $\pm$ 0.0035		0
ε_2 (^{0})	0.0157 $\pm$ 0.0034		0
ε_3 (^{0})	9.8894 $\pm$ 0.7059	14.9356740±0.0000005W	14.8 $\pm$ 5W

Several conclusions could be inferred from the tabulated values. In what follows, they are going to be analyzed in order of their level of importance.

1) Semi-axes of the triaxial ellipsoid $(\overline{a}, \overline{b}, \overline{c})$. Obviously, the three most important parameters of the fitted triaxial ellipsoid are the semi-axes. Our results show good consistency with the values previously published by Burša (1970), which are almost identical to the results recently made available by Panou et al. (2020). In this respect, it should be pointed out that the conceptual methodology used by Burša and Panou et al. is very similar except that the latter incorporated into their calculations contemporary geoid models. Keeping this in mind is not surprising that they reached similar results. However, the procedure implemented here departs from the other two because instead of using geoid undulations as observations Cartesian coordinates directly derived from the latest IERS solution: ITRF2014 were employed. Nevertheless, as the reader

can attest, the answers are sufficiently close to considering them physically plausible. Perhaps it could be speculated that the detected reasonable discrepancies are mainly caused by the variants in methodology introduced in this research for determining the best fitting triaxial ellipsoid. Among all geoid models used by Panou et al. (2020), the comparisons should concentrate on their solution "D2.1, G-T6 I" that best fit the triaxial ellipsoid to the EGM2008 geoid model undulations which is the model used in our investigation. If one contrasts the last two results in Table 1, both reinforced by cutting-edge geospatial data-bases and modern advances in digital and computational software, one finds the following differences (Soler and Han minus Panou et al.): $\delta\overline{a} = 15.32$ m; $\delta\overline{b} = -9.72$ m; and $\delta\overline{c} = 11.36$ m. In the authors' opinion, these differences should not be considered significant amid the complexity of the problem at hand and merely convey the distinct methodologies between the two procedures. The results of this investigation produces a triaxial ellipsoid which shape has slightly less rotational symmetry and polar flattening that the one from Panou et al. (2020). Perhaps with more optimum symmetric global coverage of ITRF2014 stations, our results could be improved further and better approximation, or not, to those of Panou et al. (2020) and Burša could be validated. However, at present, this is merely a postulated hypothesis difficult to be confirmed until more station coordinates data becomes available.

Finally, it is important to emphasize at this juncture that Burša's values were not used as initial approximations at any stage of the least-squares process. The original approximations of the parameters of the coefficients in equation (2) were set to zero during the first iteration.

2) Rotation angles $(\varepsilon_1, \varepsilon_2, \varepsilon_3)$. The second main resultant product to the fitting of a cluster of 3D points $(x, y, z)_G$ to a quadric surface, in particular a triaxial ellipsoid, is the spatial orientation of the ellipsoid such as the general example depicted in Fig. 5. The ellipsoid in question is randomly located in space, having its center (CE), generally speaking, not coinciding with the origin of the (x, y, z) terrestrial frame and with its coordinate axes (x_E, y_E, z_E) initially aligned with the three semi-axes also arbitrarily oriented in space (see Fig. 5). The precise spatial position of the ellipsoid is facilitated by the knowledge of the values of three rotations (positive counterclockwise) denoted $(\varepsilon_1, \varepsilon_2, \varepsilon_3)$ respectively performed around the three Cartesian axes of

the frame (x_E, y_E, z_E). Notice that these rotations are passive rotations (Soler 2018) meaning that the axes rotate and the ellipsoid remains fixed in space. The rotations by amounts $(\varepsilon_1, \varepsilon_2, \varepsilon_3)$ about the axes (x_E, y_E, z_E) are performed until they achieve a position of parallelism with respect to the geocentric (x, y, z) terrestrial frame. These three rotations will physically determine the orientation of the semi-axes in space. The values of these rotations are calculated as a function of the unequivocal components of the eigenvectors using equations. (12). For example, the rotation about the third axis is $\varepsilon_3 = 9.8894^0 \pm 0.7059^0$. Because this is a counterclockwise rotation around the z_E axis after achieving parallelism with the (x, y, z) geocentric frame, it means that the $\bar{a}$ axis (which, as mentioned before, is fixed with the ellipsoid in space) is located approximately at an angle of 9.8894^0 in a direction opposite to the rotation, that is, west of the $//x_E$ axis. The same logic could be applied to understand the physical meaning of the other two rotations ε_2 and ε_3.

3) Coordinates of the center of the ellipsoid (x_0, y_0, z_0). As Fig. 5 shows, in general, the center of the ellipsoid (CE) should not necessarily coincide, in a LS sense, with the origin of the frame defined by the cluster of $(x, y, z)_G$ points. It must be stressed here that in Burša (1970) was implicitly assumed that his triaxial ellipsoid was geocentric. Our research also solved for the shifts of the origin of the ellipsoid on the frame defined by the corresponding collection of $(x, y, z)_G$ observations that should be considered a realization of the ITRF2014 frame. As previously explained, these shifts are a byproduct of the solution of the general quadric equation and were determined afterwards through the implementation of equation (3). It is axiomatic to think that the three shifts should be primarily affected by the global symmetry of the observational data. That is, if the set of points $(x, y, z)_G$ was completely symmetric with respect to the origin of the (x, y, z) frame, the origin of the fitted ellipsoid will likely be centered at the origin of the frame. This is perfectly seen in the exercise presented in Soler et al. (2020) where the coordinates of the given points are biased by certain amounts and this is directly reflected on the solution of the shifts. With the set of coordinates at our disposal in the present case, from Table 3 one gets the following ellipsoid center displacements: $x_0 = -2.05 \text{ m} \pm 1.42$

m; y_0 =3.01 m ± 1.41 m; z_0 = 7.52 m ± 1.32 m. This appears to indicate that the distribution of points between the northern and southern hemispheres is distinctively more asymmetric than any other distribution. For example, to clarify this concept, a geoid which figure is slightly pear-shaped in the north-south direction will conceivably support a non-geocentricity shift along the z component. It is not simply that the norther hemisphere may have more stations than the southern hemisphere as Fig. 1 appears to indicate but that, overall, the geoid heights on the northern hemisphere are slightly larger than the ones in the southern hemisphere.

LS with ellipsoid shifts constrained to zero

Considering that the values of the shifts could be easily constrained to zero, an alternative LS solution was implemented, forcing the values of (x_0, y_0, z_0) to zero. This is readily done by assuring that in equation (2) $g = h = i = 0$. The results of this constrained adjustment are presented in Tables 4 and 5. The asterisks in both tables indicate that the corresponding parameters were constrained to zero.

Table 4. Parameter estimates using the ITRF2014 stations for the case of constraining $g = h = i = 0$

Parameters	Estimates [$\times 10^{-13}$]
a	0.24581350 ± 0.00000016
b	0.24582049 ± 0.00000014
c	0.24747249 ± 0.00000011
d	0.00000115 ± 0.00000010
e	-0.00000062 ± 0.00000008

f	$-0.00000125 \pm 0.00000008$
g	0*
h	0*
i	0*
Root-mean-squared distances (m)	20.2915

Table 5. Ellipsoidal parameters ($\pm 1\,\boldsymbol{\sigma}$) derived from the constrained solutions in Table 3

Parameters	This study	Burša Ellipsoid
x_0 (m)	0.0000 ± 0.0000*	0
y_0 (m)	0.0000 ± 0.0000*	0
z_0 (m)	0.0000 ± 0.0000*	0
$\overline{a}$ (m)	6378187.7495 ± 3.9840	6378173.0000 ± 10.0000
$\overline{b}$ (m)	6378092.2282 ± 3.7801	6378105.1518 ± 16.2088
$\overline{c}$ (m)	6356770.5975 ± 2.8694	6356754.3618 ± 10.0125
ε_1 (^{0})	-0.0461 ± 0.0028	0
ε_2 (^{0})	0.0143 ± 0.0027	0
ε_3 (^{0})	9.1338 ± 0.7083	$14.8^0 \pm 5^0$ W

The resulting values forcing the shifts of the origin of the ellipsoid to zero are presented in columns form in Tables 5 and 6 using the same format that the unconstrained case. Furthermore, the results of this constrained LS adjustment solution unequivocally show a slight increase on the root-mean-squared distance from the observation points to the surface of the fitted ellipsoid. This may indicate that the observations do not fit the model as well when the ellipsoid is forced to be geocentric. Thus, it can be inferred that the best triaxial earth ellipsoid fitted to the observed geospatial data at locations on the geoid is not necessarily geocentric. Indeed, although the shifts are not significantly large, the change in position of the ellipsoid also generates small changes in its orientation. The semi-axes remain practically unchanged, they are actually (constrained minus unconstrained): $\delta\overline{a} = 0.45$ m; $\delta\overline{b} = -0.10$ m; and $\delta\overline{c} = 7.00$ m. Except for the semi-minor axis $\overline{c}$ which absorbs a change of about 7m away from the Burša value to compensate for constraining the ellipsoid to be geocentric thus eliminating a shift of about 7m along the third axis. This corroborates that the values of the coordinates used are very accurate whereas imposing the geocentricity of the ellipsoid will not fit equally well the observations and gives the worst value for the third semi-minor axis. In conclusion, the results obtained by the general LS adjustment hints to an earth's best fitting triaxial ellipsoid that is not perfectly geocentric.

Additionally, after imposing the triaxial ellipsoid to be geocentric, and implementing the LS constrained solution, the rotation angle about the third axis does not change by much. This confirms, somewhat, that the semi-major axis of the best fitting triaxial ellipsoid to the irregular undulating surface of the geoid is located, approximately, parallel to the *x-y* plane, shifted by about 7m from the origin of the terrestrial frame at an angle of about 10 degrees of longitude west from the zero-meridian.

Rotations attributes

Under the assumption that the general unconstrained LS solution, as listed in Table 3, is more realistic than the one fixing to zero the coordinates of the origin of the ellipsoid, a few words will be said about the rotation results. Burša (1970) is credited with calculating, for the first time, as a function of the earth's spherical harmonics derived from early satellite observations the orientation of the equatorial semi-major axis of a triaxial best-fitting ellipsoid. From this dynamical solution, he obtained a value for the longitude of the semi-major axis of $-14.8^{\circ} \pm 5^{\circ} \equiv 14.8^{\circ} W \pm 5^{\circ}$. Later, Burša (1977), reintroduced the following equations borrowed from Darwing (1877) giving the rotations about the three axes according to the equations:

$$\delta\alpha_1 = \frac{D}{C-B}\ ;\ \delta\alpha_2 = \frac{E}{A-C}\ ;\ \delta\alpha_3 = \frac{F}{B-A} \tag{22}$$

where A, B, and C, are the earth's moments of inertia and D, E, and F are its products of inertia. Expressing these values as a function of the best spherical harmonics determined from satellite observations at that time (GEM 5 and GEM 6) Burša arrived at a value of $\delta\alpha_3 = -14.8^{\circ}$. Therefore, he proved that the angle he had previously published roughly coincided with the orientation of the principal semi-major axis of the Earth inertia ellipsoid. Subsequently, other authors corroborated this figure. For example, Soler and Mueller (1978) rigorously solving for the eigenvalues and eigenvectors of the earth's second-rank inertia tensor also determined from satellite observations, the orientation of the earth first principal inertia axis as $\delta\alpha_3 = -14^{\circ}\,55'$. More recently, following slightly different analytical methods, Groten (2007), Vîlcu (2009), and Chen and Shen (2010) reached practically the same conclusions.

The point we are trying to convey here is that all of these longitudinal angular values are referred to the orientation of the earth's first principal inertia axes, and that this is not exactly equivalent to determine the best fitting triaxial ellipsoid to the earth, or more specifically, the best fitting ellipsoid to the EGM2008 geoid model. The principal moments of inertia are affected by the total mass distribution of the earth. The irregular surface of the geoid is also affected by mass distributions; however, there is not any known theory to rigidly tie the physical shape of the geoid (materialized by its undulations) with the earth’s major principal axes of inertia. This is an area that should be investigated further. Nevertheless, it appears that the semi-major axis of the earth’s best fitting terrestrial triaxial ellipsoid is approximately oriented in the same regional area that the earth’s major principal axis of inertia, at least the historical research proves that.

Recapitulating, nobody has yet attempted an investigation along the premises presented in this article where the earth’s triaxial ellipsoid is fitted to a collection of Cartesian points accurately located on the ITRF2014 frame. From the values in Table 3 containing the unconstrained solution, it can be deduced that the third axis of the physically fitted ellipsoid will approximately be located at a spherical curvilinear distance of only 4.68 km from the north pole of the ITRF2014 frame along the meridian of longitude 240.6963°. Recall that this axis has only geometric meaning and is not directly related to the instantaneous rotation axis of the earth or its third principal inertia axis.

Actually, because the rotations around the first and second axes are close to zero, the rotation around the third axis comprises an angle of about 10° (in our solution) that can be translated into the plane of the equator of the triaxial ellipsoid. However, the rigorous computation of this angle will require the solution of a spherical triangle (see Appendix II). In Fig. A1, the three positive counterclockwise rotations about their corresponding axis are shown. The figure depicts the last sequence of a rotation ε_2 about the second axis followed by the final rotation ε_3 about the third axis. Notice that, at this point, the axes y_E and z_E have changed the location pictured in the figure. Of our interest is the spherical triangle α drawn in the figure. This is the angle in space between the axis parallel to the geocentric x-axis and the location of the semi-mayor axis $\bar{a}$ of the triaxial ellipsoid. Using standard spherical trigonometry and following the steps outlined in Appendix II (Fig. A2) one reaches the answer $\alpha = 9.8994^{\circ} \approx 10^{\circ}$. Consequently, the true angle that one is after is 9.8994° versus the value of the rotation about the third axis $\varepsilon_3 = 9.8894^{\circ}$ directly determined in the least-squares solution of Table 3. The difference between both is so small because the values of the other two rotations ε_1 and ε_2 are very close to zero. Although the result is practically identical, the intention of the authors was to emphasize the rigorous mathematical discrepancy between the two angular solutions considering that this distinction is never treated in all discussions related to the fitting of earth's triaxial ellipsoids. One thing is to resolve the orientation of the triaxial ellipsoid in space through the determination of three rotation angles and the other to publish the angle between the semi-major axis with respect to the geocentric (terrestrial) x-axis. Therefore, to mention simply that the semi-major axis is 14° W $= -14^{\circ}$ is not 100% correct. This assertion is only rigorous if the other two rotation angles are zero, meaning that the semi-minor axis of the triaxial ellipsoid is parallel (or coincides) with the third axis of the geocentric frame, a very singular and improbable circumstance.

Conclusions

In this investigation, a set of 3D Cartesian coordinates given in the ITRF2014 frame at geodetic stations located on the surface of the EGM2008 geoid model were used to fit a triaxial ellipsoid after implementing a LS procedure. A trivial scheme was devised to "reduce from terrain to geoid" the coordinates that were primarily based on the computation of orthometric heights (H) from the rigorous knowledge of the geodetic height h and the value of the undulation of the geoid N $(H \approx h - N)$. Results comparable to previous investigations dating back about 50 years were reached. However, the procedure developed for the preparation of this work is different from the preceding aforementioned research. While other authors have used the undulations of modeled geoids as observations, our research uses 3D rigorous, up-to-date geospatial-determined Cartesian coordinates as observables. Nevertheless, it should be pointed out that, as in previous investigations, possible errors in the undulations of the geoid models (EGM2008 in our case) may affect the results. Consequently, in this research, an upper bound of $H < 500$ m was enforced to reduce, as much as feasible, unknown uncertainties on the values of the undulations. Concentrating now on the findings obtained for the best fitting triaxial ellipsoid, the reader is addressed to Table 3. The general LS solution gives the following results involving 1163 ITRF2014 stations disseminated around the world: for the three semi-axes: $\bar{a}$ = 6378187.20m ± 3.97m, $\bar{b}$ = 6378092.3m ± 3.92m, $\bar{c}$ = 6356763.60m ± 3.78m; for the three shifts x_0 = −2.05 ± 1.42m, y_0 = 3.01m ± 1.41m, z_0 = 7.52m ± 1.32m; and for the three rotations ε_1 = −0.0447° ± 0.0035°, ε_2 = 0.0157° ± 0.0034°, ε_3 = 9.8894° ± 0.7059°.

Because the results might be slightly dependent on the distribution of points on the earth surface, in the future, when some of the geographic regions in Fig. 2 that currently lack ITRF2014 points, e.g. northern Siberia, central Africa, and Antarctica, are filled, the outcomes presented herein could be improved. This enhancement should advance further the scientific knowledge of the best closed mathematical expression of our planet.

It has been found that the entire methodology is founded, at least, on two demanding premises, a general LS solution and a rigorous eigentheory determination of the variance-covariance matrix of the semi-axes and rotations of the fitted triaxial ellipsoid. As far as the authors' are concerned, no approach scientifically equivalent to the one introduced here has been published or attempted to date. On the contrary, the standard procedure to determine the best earth's triaxial ellipsoid through the years follows the path of the innovative ideas advanced by Burša originally in 1970. Our proposal appears to be a viable alternative but lacks the availability of a denser network of geodetic stations around the world. It is plausible to speculate that in the course of time, this existent weakness will be strengthened and, without any doubt, it can be predicted that much better, improved and accurate results could be attained.

Acknowledgment

The authors would like to thank the two anonymous reviewers for their constructive comments, which significantly improved the quality of the original manuscript.

Data Availability

Data containing the station coordinates and their standard deviations used in this study were obtained from the SINEX files publicly available at the ITRF web site http://itrf.ensg.ign.fr/ITRF_solutions/2014/ITRF2014_files.php. Processing logs and result files are available from the corresponding author on reasonable request.

References

Altamimi Z, Rebischung P, Métivier L, Collilieux X (2016) ITRF2014: a new release of the International Terrestrial Reference Frame modeling nonlinear station motions. J Geophys Res 121(8): 6019-6131. https://doi.org/10.1002/2016JB013098

Bachmann S, Messerschmitt L, Thaller D (2015), IVS contribution to ITRF2014, in IAG Commission 1 Symposium 2014: Reference Frames for Applications in Geosciences (REFAG2014), pp. 1–6, Springer, Berlin.

Bektaş Š (2014) Orthogonal distance from an ellipsoid. Bol Ciênc Geod 20(4): 970-983. https://doi.org/10.1590/S19 82-21702014000400053

Bektaş Š (2015) Least squares fitting of ellipsoid using orthogonal distances. Bol Ciênc Geod 21(2): 329-339. https://doi.org/10.1590/S1982-21702015000200019

Burša M (1970) Best-fitting tri-axial earth ellipsoid parameters derived from satellite observations. Stud Geophys Geod, 14(1): 1-9. https://doi.org/10.1007/BF02585546

Burša M (1971) On the triaxiality of the earth on the basis of satellite data. Stud Geophys Geod, 15(3-4): 228–240. https://doi.org/10.1007/BF01589239

Burša M, Pícha J (1972) Fundamental geodetic parameters of the earth's figure and the structure of the earth's gravity field derived from satellite data. Stud Geophys Geod 16(1), 10–29. https://doi.org/10.1007/BF01614229

Burša M (1977) Positions of the axes of the ellipsoid of Inertia from satellite observations. Bull Astron Inst Czechoslovakia, 28: 316

Burša M, Šíma Z (1980) Triaxiality of the Earth, the Moon and Mars. Studia Geophys Geod 24(3): 211–217

Burša M, Fialová V (1993) Parameters of the earth's tri-axial level ellipsoid. Studia Geophys Geod, 37(1): 1-13. https://doi.org/10.1007/BF01613918

Chen W, Shen W (2010) New estimates of the inertia tensor and rotation of the triaxial nonrigid earth. J Geophys Res, 115(B12)

Darwin GH (1877) On the influence of geological changes on the earth's axis of rotation. Phil Trans Royal Soc A (167): 271-312. Also in Scientific Papers, 1910, III: 1-46. Cambridge University Press

Diaz-Toca GM, Marin L, Necula I (2019) Direct transformation from Cartesian into geodetic coordinates on a triaxial ellipsoid. arXiv preprint arXiv:1909.06452

Drummond J, Christou J (2008) Triaxial ellipsoid dimensions and rotational poles of seven asteroids from Lick Observatory adaptive optics images, and of Ceres. Icarus 197(2): 480-496

IERS Message 103 (2006) http://www.iers.org/documents/ac/sinex/ sinex_v202.pdf.

Eitschberger B (1978) Ein Geodätisches Weltdatum aus terrestrischen und Satellitendaten (A Geodetic World Datum from Terrestrial and Satellite Data) Ph.D. Thesis - Bonn Univ, Deut Geodaetische Komm no 245, pp 188

Geodetic Glossary (1986) Publication of the National Geodetic Survey (NGS), NOAA/NOS, National Geodetic Information Center, Rockville, MD, pp 71

Grafarend EW, You R-J, Syffus R (2014) Map Projections: Cartographic Information Systems, 2nd ed. Springer, New York, pp 864

Han J-Y, van Gelder BHW, Soler T (2007) On covariance propagation of eigen-parameters of symmetric n-D tensors. Geophys J Int, 170(2): 503-510.

Krasovsky FN (1902) Determination of the size of the earth triaxial ellipsoid from the results of the Russian arc measurements. Memorial book of the Konstantinovsky Surveying Institute for the 1900–1901 years, 19-54 (in Russian)

Krasovsky FN (1972). Triaxial ellipsoid values reported in Geodetic Glossary (1986)

Leick A, Rapaport L, Tatarnikov D (2015) GPS Satellite Surveying 4th ed., John Wiley and Sons, Inc, New York, NY.

Luceri V, Pavlis E (2016), The ILRS contribution to ITRF2014. [Available at http://itrf.ign.fr/ITRF_solutions/2014/doc/ILRS-ITRF2014-description.pdf.]

Moreaux, G, Lemoine FG, Capdeville H, Kuzin S, Otten M, Stepanek P, Willis P, Ferrage P (2016), Contribution of the International DORIS Service to the 2014 realization of the International Terrestrial Reference Frame, Adv. Space Res., 63(1), 118-138 doi:10.1016/j.asr.2015.12.021.

Moritz H (1992) Geodetic reference system 1990. Bull Géod 66(2): 187-192

Panou G, Agatza-Balodimou A-M (2020) Direct and indirect estimation of the variance-covariance matrix of the parameters of a fitted ellipse and a triaxial ellipsoid. ResearchGate (Preprint), pp 19

Panou G, Korakitis R, Pantazis G (2020) Fitting a triaxial ellipsoid to a geoid model. ResearchGate (Preprint), pp 21

Pavlis NK, Holmes SA, Kenyon S, Factor JK (2012) The development and evaluation of the Earth Gravitational Model 2008 (EGM2008). J Geophys Res 117, B04406.

https://doi.org/10.1029/2011JB008916

Rao CR, and Mitra SK (1971) Generalized Inverse of Matrices and its Applications, John Wiley & Sons, New York, NY.

Rebischung P, Altamimi Z, Ray J, Garayt B (2016) The IGS contribution to ITRF2014. J Geod 90(7): 611–630. https://doi.org/10.1007/s00190-016-0897-6

Schliephake G (1956) Berechnungen auf dem dreiachsigen Erdellipsoid nach Krassowski Vermessungstechnik, 4: 7-10

Soler T (2018) Active versus passive rotations. J Surv Eng 144(1): 06017004

Soler T, van Gelder BHW (1991) On covariances of eigenvalues and eigenvectors of second-rank symmetric tensors. Geophys J Int 105(2): 537-546

Soler T, van Gelder BHW (2006) Corrigendum: On covariance of eigenvalues and eigenvectors of second-rank symmetric tensors (vol. 105, pp 537-546, 1991). Geophys J Int 165(1): 382

Soler T, Mueller II (1978) Global plate tectonics and the secular motion of the pole. Bull Géod 52(1): 39-57.

Soler T, Han J-Y, Huang CJ (2020) Estimating the variance-covariance matrix of the parameters of a fitted triaxial ellipsoid. J Surv Eng 146(2), 04020003.

Teunissen PJG (1989) First and second moments of non-linear least-squares. Bull Géod 63(3): 253–262

Vîlcu AD (2009) On the elements of the earth's ellipsoid of inertia. An Univ Bucuresti Mat, 58(2): 183–198

Zhuravlev SG (1972) Stability of the libration points of a rotating triaxial ellipsoid. Celestial Mech, 6(3): 255-267.

<u>Appendix I</u>. A practical example of the Khatri–Rao product

Assume that one wants to compute the following Khatri-Rao product, as it appears in (15),

$$\underset{3\times3}{[E]^T} \square \underset{3\times3}{[E]^T} \tag{A.1}$$

where $[E]$ is the following matrix of eigenvectors:

$$[E] = \begin{bmatrix} e_{11} & e_{12} & e_{13} \\ e_{21} & e_{22} & e_{23} \\ e_{31} & e_{32} & e_{33} \end{bmatrix} \Rightarrow [E]^T = \begin{bmatrix} e_{11} & e_{21} & e_{31} \\ e_{12} & e_{22} & e_{32} \\ e_{13} & e_{23} & e_{33} \end{bmatrix} = \begin{bmatrix} \begin{Bmatrix} e_{11} \\ e_{12} \\ e_{13} \end{Bmatrix} & \begin{Bmatrix} e_{21} \\ e_{22} \\ e_{23} \end{Bmatrix} & \begin{Bmatrix} e_{31} \\ e_{32} \\ e_{33} \end{Bmatrix} \end{bmatrix} \tag{A.2}$$

Then, by definition:

$$\underbrace{\underset{3\times3}{[E]^T} \square \underset{3\times3}{[E]^T}}_{9\times3} = \begin{bmatrix} e_{11}\begin{Bmatrix} e_{11} \\ e_{12} \\ e_{13} \end{Bmatrix} & e_{21}\begin{Bmatrix} e_{21} \\ e_{22} \\ e_{23} \end{Bmatrix} & e_{31}\begin{Bmatrix} e_{31} \\ e_{32} \\ e_{33} \end{Bmatrix} \\ e_{12}\begin{Bmatrix} e_{11} \\ e_{12} \\ e_{13} \end{Bmatrix} & e_{22}\begin{Bmatrix} e_{21} \\ e_{22} \\ e_{23} \end{Bmatrix} & e_{32}\begin{Bmatrix} e_{31} \\ e_{32} \\ e_{33} \end{Bmatrix} \\ e_{13}\begin{Bmatrix} e_{11} \\ e_{12} \\ e_{13} \end{Bmatrix} & e_{23}\begin{Bmatrix} e_{21} \\ e_{22} \\ e_{23} \end{Bmatrix} & e_{33}\begin{Bmatrix} e_{31} \\ e_{32} \\ e_{33} \end{Bmatrix} \end{bmatrix} = \begin{bmatrix} e_{11}^2 & e_{21}^2 & e_{31}^2 \\ e_{11}e_{12} & e_{21}e_{22} & e_{31}e_{32} \\ e_{11}e_{13} & e_{21}e_{23} & e_{31}e_{33} \\ e_{12}e_{11} & e_{22}e_{21} & e_{32}e_{31} \\ e_{12}^2 & e_{22}^2 & e_{32}^2 \\ e_{12}e_{13} & e_{22}e_{23} & e_{32}e_{33} \\ e_{13}e_{11} & e_{23}e_{21} & e_{33}e_{31} \\ e_{13}e_{12} & e_{23}e_{22} & e_{33}e_{32} \\ e_{13}^2 & e_{23}^2 & e_{33}^2 \end{bmatrix} \tag{A.3}$$

<u>Appendix II</u>. **Direct angle between the semi-major axis of the fitted triaxial ellipsoid and the //*x* axis**

When solving for the orientation of the semi-major axis of the triaxial ellipsoid, the angle that should be reported is not ε_3 but α depicted in the right angle spherical triangle of Fig. A1.

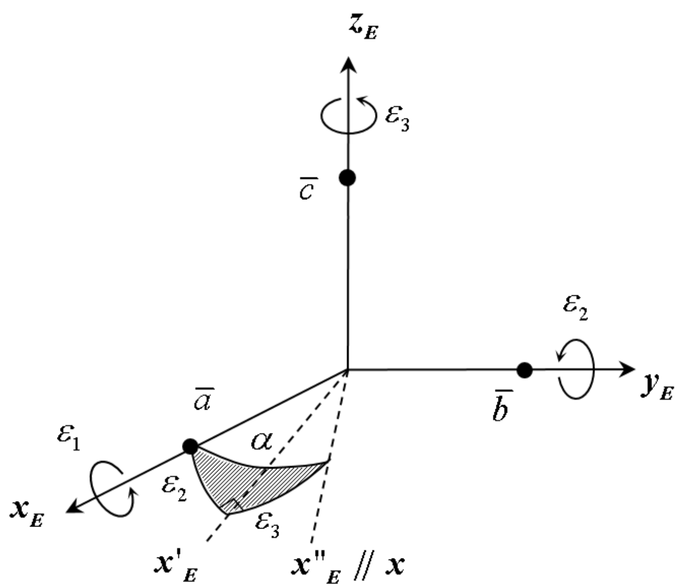

Fig. A1. Relationship between rotation angles and the angle α between the semi-major axis $\overline{a}$ and the □ $\boldsymbol{x}$ axis

According to the well-known Napier's rules (Fig. A2):

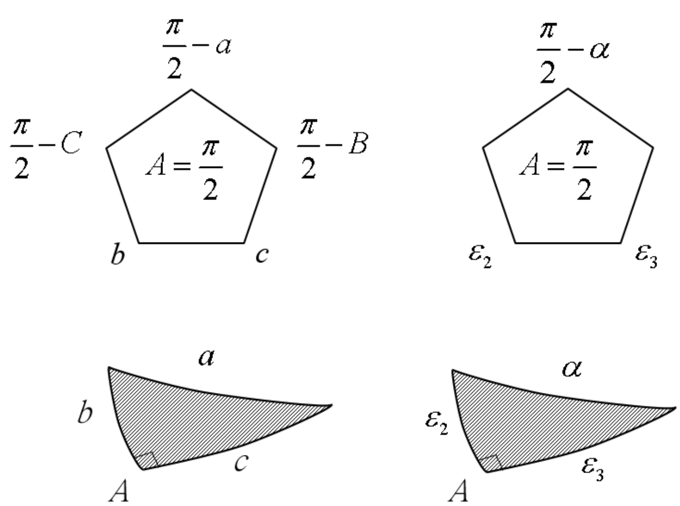

Fig. A2. Practical solution of right angle spherical triangles

$$\sin\left(\text{middle part}\right) = \cos\left(\text{opposit part}\right) \times \cos\left(\text{opposit part}\right) \tag{A.4}$$

Consequently,

$$\sin\left(\frac{\pi}{2} - \alpha\right) = \cos\varepsilon_2 \times \cos\varepsilon_3 \Rightarrow \cos\alpha = \cos\varepsilon_2 \times \cos\varepsilon_3 \tag{A.5}$$

$$\alpha = \cos^{-1}\left(\cos\varepsilon_2 \times \cos\varepsilon_3\right) \tag{A.6}$$

And after substituting $\varepsilon_2 = 0.0157^0$ and $\varepsilon_3 = 9.8894^0$ in equation (A.6) one finally gets the angle between the semi-major axis and the axis $//x$ equal to: $\alpha = 9.8994^0 \approx 10^0$.

Author Biography

Tomás Soler holds a Ph.D. from The Ohio State University. He worked at the National Geodetic Survey a federal agency located within the National Oceanic and Atmospheric Administration (NOAA), Silver Spring, MD, until his retirement in 2017. He continues to investigate a variety of theoretical and applied research topics related to geodesy.

Jen-Yu Han received a Ph.D. degree in Civil Engineering from Purdue University, USA and is a Professor at the Civil Engineering Department at National Taiwan University, Taipei, Taiwan. He also serves as the Duty Director at the NRCEE-NTUCE Joint AI Research Center. His research interests include geodetic reference frames, error theory, deformation analysis, lidar system, and intelligent image sensors.